Role of Oxygen Deposition Pressure in the Formation of Ti Defect States in TiO$_2$(001) Anatase Thin Films

Benoit Gobaut,*[†,††] Pasquale Orgiani,[‡] Alessia Sambri,[§,∥] Emiliano di Gennaro,[§,∥] Carmela Aruta,[§,∥] Francesco Borgatti,[⊥] Valerio Lollobrigida,[#] Denis Céolin,[¶] Jean-Pascal Rueff,[¶,▽] Regina Ciancio,[#] Chiara Bigi,[#,○] Pranab Kumar Das,[#,◆] Jun Fujii,[#] Damjan Krizmancic,[#] Piero Torelli,[#] Ivana Vobornik,[#] Giorgio Rossi,[#,○] Fabio Miletto Granozio,[§,∥] Umberto Scotti di Uccio,[§,∥] and Giancarlo Panaccione[#]

[†]Elettra Sincrotrone Trieste S.c.p.A., Basovizza, I-34012 Trieste, Italy
[‡]CNR—SPIN, UOS Salerno, I-84084 Fisciano, Italy
[§]CNR—SPIN, UOS Napoli, I-80126 Napoli, Italy
[∥]Department of Physics, University of Napoli Federico II, I-80126 Napoli, Italy
[⊥]CNR—ISMN, UOS Bologna, I-40129 Bologna, Italy
[#]CNR—IOM, Laboratorio TASC, I-34149 Trieste, Italy
[¶]Synchrotron SOLEIL, L'Orme des Merisiers, BP 48, Saint Aubin, 91192 Gif sur Yvette, France
[▽]Laboratoire de Chimie Physique-Matière et Rayonnement, UPMC Université; Paris 06, CNRS, UMR 7614, F-75005 Paris, France
[○]Department of Physics, University of Milano, I-20133 Milano, Italy
[◆]International Centre for Theoretical Physics (ICTP), I-34100 Trieste, Italy

Ⓢ *Supporting Information*

ABSTRACT: We report the study of anatase TiO$_2$(001)-oriented thin films grown by pulsed laser deposition on LaAlO$_3$(001). A combination of in situ and ex situ methods has been used to address both the origin of the Ti^{3+}-localized states and their relationship with the structural and electronic properties on the surface and the subsurface. Localized in-gap states are analyzed using resonant X-ray photoelectron spectroscopy and are related to the Ti^{3+} electronic configuration, homogeneously distributed over the entire film thickness. We find that an increase in the oxygen pressure corresponds to an increase in Ti^{3+} only in a well-defined range of deposition pressure; outside this range, Ti^{3+} and the strength of the in-gap states are reduced.

KEYWORDS: anatase, oxygen vacancies, resonant photoemission, in-gap state, shear planes, interdiffusion, defects
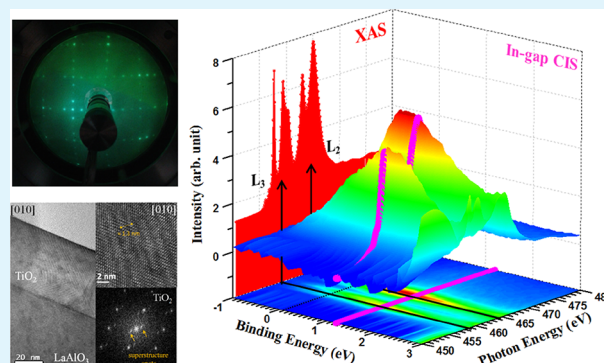
1. INTRODUCTION

Titanium dioxide (TiO$_2$) is one of the most widely studied oxides because of its specific surface properties,[1−3] making it a good candidate for photocatalysis of water[4] and for reducing gas pollutants for air and water treatment,[5,6] and its photoinduced hydrophilic properties.[7,8] Thin films of TiO$_2$ are also the subject of interest for photovoltaic applications[9] or resistive switching memory devices.[10,11] TiO$_2$ is present in nature in three different polymorphs: rutile, anatase, and brookite. Although the most stable form under ambient conditions is rutile, the quasi-metastable anatase TiO$_2$ is considered to be potentially more relevant for energy-related applications.[12−20]

TiO$_2$ anatase is an insulator with a band gap of 3.2 eV;[21,22] however, changes in the concentration of oxygen vacancies (TiO$_{2−δ}$) influence the value of the band gap. Calculations have

shown that the oxygen vacancies act like donors in the n-type semiconductor.[23] This results in the formation of Ti^{3+}-related electronic states located in the band gap. Localized in-gap states may overlap with the electronic states at the conduction band minimum (CBM), eventually reducing the value of the gap.[24] The mobility of charge carriers being determined by the defect concentration, it is now well-understood that the carrier dynamics is largely influenced by the space charge layer and defect states on the surface and subsurface regions.[25,26] Knowing that many TiO$_2$ relevant properties are linked to the origin and evolution of Ti^{3+} defect states, a deeper understanding of the surface versus bulk properties and of

surface chemistry is mandatory.[27−31] In particular, low electron mobility in devices often represents the bottleneck of overall performances;[16] thus, the formation of electronic in-gap states and their homogeneous (or not) distribution over depth are crucial parameters for future applications.[32]

Thin film growth technology[33,34] now enables tuning the growth conditions of TiO_2 anatase films of different thicknesses and oxygen contents. Recent reports have combined scanning probe techniques[35−37] and X-ray spectroscopy measurements[38−42] to investigate the origin and arrangement of Ti^{3+} defect states in films.

Here, we have analyzed the structural and electronic arrangement of TiO_2(001)-oriented anatase thin films with different oxygen contents ($TiO_{2−\delta}$). First, a very accurate characterization of our samples from the viewpoint of film growth, crystal structure, and surface quality was performed. Transmission electron microscopy (TEM) experiments provided evidence of regular oxygen vacancies shear planes uniformly distributed over the entire film thickness in a highly crystalline environment. Reflective high-energy electron diffraction (RHEED), low-energy electron diffraction (LEED), scanning tunneling microscopy (STM), and X-ray diffraction (XRD) characterizations contribute to show that our pulsed laser deposition (PLD)-grown samples, while hosting point defects giving rise to in-gap states whose nature is addressed in the following, show an excellent long-range order and a very high overall quality. Depth-sensitive photoemission spectroscopy (PES) results are able to (i) disentangle the contribution of different Ti ionic states (Ti^{4+} and Ti^{3+}), (ii) monitor the (homogeneous) diffusion of Al from the substrate through the film, and (iii) reveal the distribution of Ti^{3+} versus depth. Resonant photoelectron spectroscopy (ResPES) with polarized synchrotron radiation has been used to identify the in-gap defect states as related to Ti states only. By exploiting the PES sensitivity to the electronic state symmetry, we have been able to demonstrate a direct correlation between Ti^{3+} ions and the intensity of in-gap states. Contrary to what is generally expected, our results demonstrate that a direct proportionality between the oxygen deposition pressure and the amount of Ti^{3+} holds only in a well-defined range of deposition pressure. These findings suggest that not only the Ti^{3+} ions content can modulate the population of the in-gap states but also a control on such gap states is achievable. This acquired capability is a strong basis for tailoring the electronic properties of TiO_2 anatase thin films for applications in oxide electronics and catalysis.

2. EXPERIMENTS

2.1. Growth and Structural Characterization. Samples of TiO_2 were grown by PLD using a KrF excimer pulsed laser source (λ = 248 nm) at a typical energy density of about 2 J/cm^2 and a typical laser repetition rate of 1 Hz. The growth temperature was set to 700 °C, and the target−substrate distance was about 5 cm. The typical deposition rate was about 5 A/min. This growth rate is thus 1 order of magnitude faster than the deposition rate described in the literature for growing stoichiometric TiO_2 samples.[37] A stoichiometric polycrystalline TiO_2 target was used for the deposition process, and the oxygen pressure was varied from 10^{-5} to 10^{-1} mbar. All samples were grown with a nominal thickness of 50 nm. The growth process was monitored in situ by RHEED, allowing the evaluation of the thin film surface morphology during the growth process at any oxygen pressure (i.e., up to 10^{-1} mbar). As a matter of fact, under the selected experimental conditions, the plume stopping distance becomes shorter than the target−substrate distance only for a pressure of several mbars, so that

the film deposition is possible in the entire explored pressure range. To fully exploit such a capability, high-pressure RHEED systems were used, allowing in situ monitoring of the deposition process at high pressure.

The growth was performed on (001)-oriented LAO substrates, thus ensuring an epitaxial growth along the same (001) axis of the TiO_2 film. RHEED images of a typical TiO_2/LAO film at different deposition stages are shown in Figure 1. As demonstrated by the
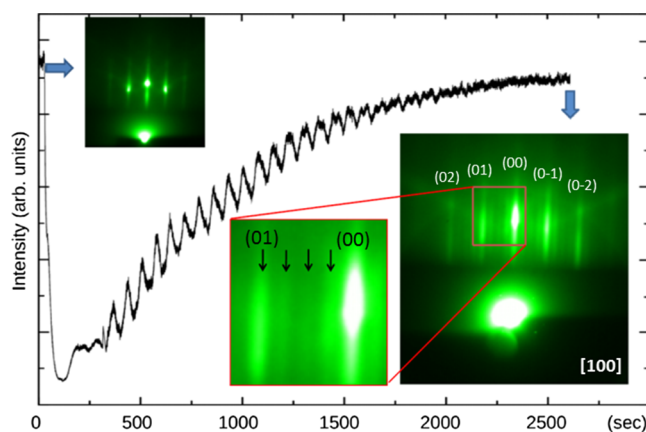

Figure 1. Typical RHEED oscillation during the TiO_2 thin film growth on the $LaAlO_3$ (LAO) substrate at 10^{-1} mbar. RHEED patterns were recorded at the beginning (i.e., bare substrate) and at the end of the deposition. In particular, the RHEED pattern at the end of the deposition showing a (4 × 1) surface reconstruction is zoomed out.

analysis of the RHEED pattern, a pure two-dimensional (2D) termination of the bare LAO substrate was observed. At the initial stage of deposition, the RHEED-diffracted specular spot oscillated according to a pure layer-by-layer growth mode to finally turn into a 2D step-flow growth mode. Such a transition, which has been also observed in other complex perovskite materials,[43] does not affect the dimensionality of surface termination, thus preserving the high quality of the final surface. Moreover, RHEED analysis also confirms the appearance of the well-known (4 × 1) surface reconstruction, characteristic of the (001) anatase TiO_2 thin film (see arrows in the inset of Figure 1).

The bulk crystallographic properties of the grown samples were explored by means of XRD. Structural characterization was carried out using a four-circle diffractometer with a Cu Kα radiation source. A typical $\theta/2\theta$ spectrum only shows the (00l) peaks, indicating the preferential c-axis orientation of the film along the [001] substrate crystallographic direction with no trace of impurity phases (not shown here). The out-of-plane parameter has been measured to be 0.958 ± 0.001 nm, in good agreement with the expected c-axis parameter of the relaxed TiO_2 anatase. As expected by the very low lattice mismatch with the LAO substrate (0.1%), the (001) anatase TiO_2 thin films grow fully matching with the in-plane lattice parameters of the substrate.[44] Reciprocal space map around the (0−13) LAO and (0−17) TiO_2 asymmetric reflections shows a perfect alignment of the diffraction peak along the Q_x-direction, proving the full in-plane lattice matching between the film and the substrate (see Figure 2a).

The surface structural properties were studied using LEED and STM techniques.

LEED investigations (Figure S1a) of TiO_2 thin films always show an ordered (4 × 1) + (1 × 4) reconstructed surface, independent of the deposition process (i.e., oxygen content). Even though the origin of such a surface reconstruction is still debated,[45,46] its dependence upon O stoichiometry on the surface of the film is clear.[47] In situ STM was conducted using an atomic resolution ultrahigh vacuum (UHV) STM apparatus at the APE-IOM beamline at Elettra synchrotron facility in Italy,[48] immediately after the in situ growth of the samples in UHV. STM topography (Figure S1b,c) shows good surface quality with atomic steps along the main crystallographic axis [100] and [010] and
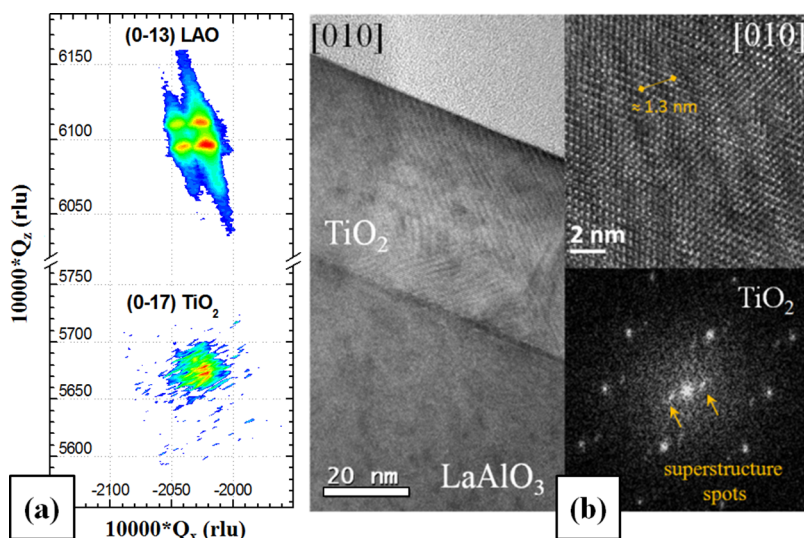
Figure 2. (a) Reciprocal space map around the (0−13)-LAO and (0−17)-TiO$_2$ asymmetric Bragg reflections. (b) High-resolution transmission electron microscopy (HRTEM) image of a TiO$_2$/LAO film grown under an oxygen pressure of 10^{-2} mbar. The image is taken in the [010] zone axis of the film showing shear planes homogeneously distributed all over the film; in the HRTEM shown in the top inset, the 1.3 nm periodicity of the crystallographic shear (CS) planes can be appreciated; in the lower inset is the diffractogram of the CS region, enlightening the presence of satellite peaks in addition to the characteristic pattern of anatase TiO$_2$.
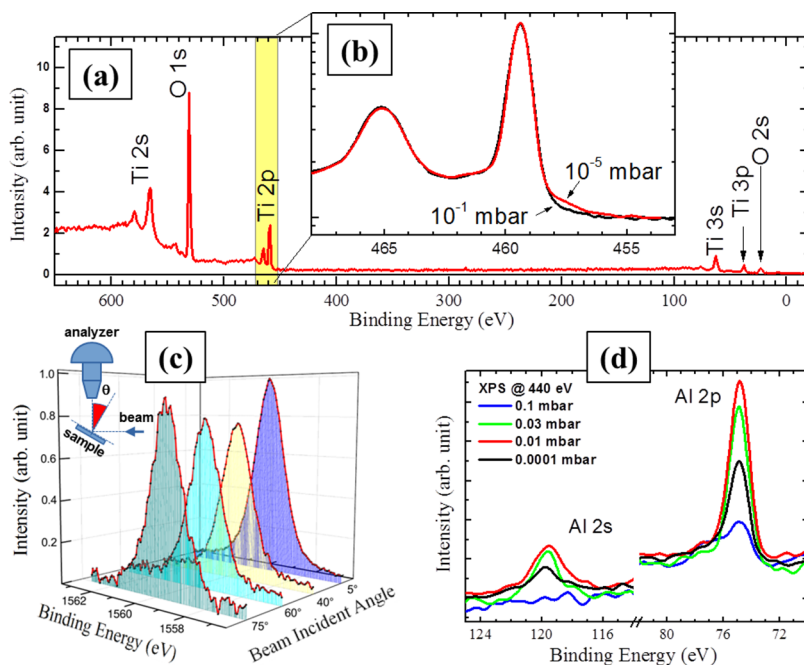

Figure 3. (a) Hard X-ray photoelectron spectroscopy (HAXPES) overview scan of a TiO$_2$/LAO sample with a photon energy of 6900 eV with all peaks labeled. (b) Zoomed-out image of the Ti 2p peak showing the Ti^{3+} shoulder around 457 eV for the sample grown at 10^{-5} mbar of oxygen pressure (red curve). (c) Al 1s X-ray photoelectron spectroscopy (XPS) peak measured at different photoelectron emission angles θ, namely, 5° (blue), 40° (yellow), 60° (cyan), and 75° (green); schematics of the beam/sample/analyzer geometry is also reported. (d) Al 2s and Al 2p peaks measured with a photon energy of 440 eV at the APE beamline (synchrotron Elettra) of the sample grown at different oxygen pressures (from 10^{-5} up to 10^{-1} mbar).

periodic structures along the same axis with a periodicity of about 1.5 nm, confirming the (4 × 1) reconstruction (visible on the zoomed-in image presented in Figure S1c).

The atomic structure of the TiO$_2$ films was investigated using HRTEM. In particular, by resorting to cross-sectional HRTEM, we revealed the presence of ordered structural defects within the film and determined their evolution across the growth direction. HRTEM experiments were performed using a TEM/STEM JEOL 2010 UHR field emission gun microscope operated at 200 kV with a measured spherical aberration coefficient C_s = 0.47 ± 0.01 mm. A representative

HRTEM image of the TiO$_2$/LAO cross-sectional area taken in the [010] zone axis of the film is shown in Figure 2b. The TiO$_2$ film has a modulated structure with regular arrays of planar faults uniformly distributed all along the film thickness. This specific structure has already been described for titanium dioxide anatase films[49,50] and related to the existence of CS planes derived from the long-order reorganization of oxygen vacancies within the film. As better emphasized in the HRTEM displayed in the top inset of Figure 2b, these planar faults exhibit a brighter contrast at the CS ridges with respect to the host matrix and have a relative distance of about 1.3 nm.
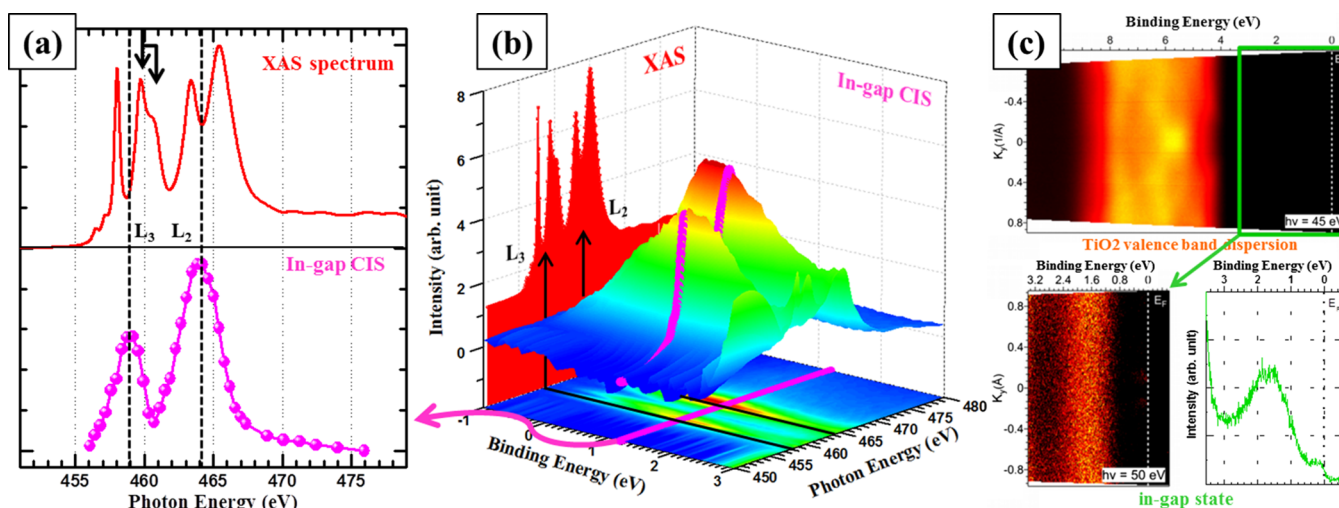
Figure 4. (a) X-ray absorption spectrum (red curve in the upper panel) and constant initial state (CIS) curve for the in-gap states at E_b = 1.8 eV as a function of the exciting photon energy (magenta line points in the lower panel). (b) ResPES map of the valence band (VB) as a function of the exciting photon energy; the X-ray absorption spectrum is also reported (red); and the energies at which the in-gap states show relative maxima (i.e., 459 and 464 eV corresponding to L_3 and L_2, respectively) are reported on the map [the energy resolution for X-ray absorption spectroscopy (XAS)/ResPES experiments was about 100 meV]. (c) Angular-resolved photoemission spectroscopy (ARPES) band dispersion of the TiO_2 thin film (upper panel) grown at 10^{-2} mbar, with a zoomed-out image of the in-gap state region (lower left) and its angular integrated dependence with respect to the binding energy (BE, lower right).

The diffractogram of the CS region displayed in the lower inset of Figure 2b shows the typical multiple-peak pattern of a Ti_nO_{2n-1} superstructure originated by the long-range ordering of the CS planes in the film.

2.2. Core-Level Spectroscopy Techniques. HAXPES experiments have been performed at the GALAXIES beamline[51] (SOLEIL synchrotron facility, France) equipped with a Scienta EW4000. HAXPES spectra were obtained at a photon energy of 2.5 keV using a Si(111) monochromator giving an overall energy resolution of 300 meV and at a photon energy of 6.9 keV where the energy resolution was up to 150 meV, thanks to the Si(333) monochromator.

In this case, samples were transferred ex situ, and no surface preparation was performed. HAXPES measurements were recorded on two (001)-oriented $TiO_2(001)$ anatase films grown by PLD on LAO at two different oxygen pressures (10^{-1} and 10^{-5} mbar). In the HAXPES regime, the high kinetic energy of the measured photoelectrons guarantees specific bulk sensitivity, with a residual surface sensitivity below a certain percentage.[52] In the survey scan of a sample grown at 10^{-5} mbar (Figure 3a), the contribution of surface contaminants is severely reduced with the C 1s peak hardly visible, despite no surface preparation. The survey spectrum shows all of the expected peaks for TiO_2. Some extra peaks (corresponding to Al 1s, Al 2s, and Al 2p) are visible (Figure 3a) both in hard and soft (more surface sensitive) XPS (Figure 3c,d). This reveals the presence of Al diffusion through the film up to the surface.[53]

To better understand the concentration of Al throughout the film, we performed angular scans, varying the depth sensitivity through a change in the detection angle (see the scheme on Figure 3c). Measurements were recorded close to normal emission (5°), that is, 40°, 60°, and up to 75° emission angles. The intensity of the Al peak is almost constant (standard deviation is in the order of 12%) with the decrease in the probing depth, thus indicating that Al is homogeneously distributed over the entire film for a fixed oxygen deposition pressure. However, the Al content depends upon the oxygen deposition pressure, as shown in Figure 3d, where soft X-ray ($h\nu$ = 440 eV) PES core level spectra of Al 2p and Al 2s are displayed. Interestingly, the overall amount of Al in the investigated TiO_2 samples is not constant, thus raising concern about a trivial Al interdiffusion process from the LAO substrates triggered by the substrate temperature during the growth, which was kept constant. As will be discussed later in the manuscript, the amount of Al appears to be directly correlated with the amount of Ti^{3+}. This also raises

questions on the origin of the Ti^{3+} electronic state, which could result from a combination of several factors, including interstitial Ti^{3+} from shear planes, extra interdiffused Al^{3+}, or oxygen vacancies.

The electronic configuration of Ti atoms in fully oxygenated TiO_2 is Ti^{4+}. The presence of a small amount of atoms in the Ti^{3+} configuration, which is usually related to O vacancies, is revealed in our samples by the small shoulder on the lower BE side of the main Ti 2p peak[54−56] (see Figure 3b). This amount clearly differs for different oxygen deposition pressures (e.g., samples grown at oxygen pressures of 0.1 and 10^{-5} mbar). Interestingly, we also performed angular scans on the Ti 2p peak to probe the distribution of the Ti^{3+} configuration within the bulk of the film, revealing a homogeneous distribution of this electronic state with the probing depth (see Figure S2).

2.3. ResPES and ARPES Experiments. Soft X-ray and ultraviolet synchrotron radiation spectroscopies (XPS, resonant photoemission spectroscopy, XAS, and ARPES) were carried out at the APE-IOM beamline at Elettra.[48] The measurements were recorded on the samples that were transferred in situ directly after growth under UHV conditions (base pressure < 2 × 10^{-10} mbar) to the two APE endstations. The energy resolution for XAS/ResPES experiments was about 100 meV, though the absolute photon energy value was not calibrated. All spectroscopic characterizations at APE were performed on the very same samples.

For XAS experiments performed in the total electron yield mode, the drain current from a highly transparent mesh was used to normalize the measured signal with the incident photon flux. XAS of the Ti $L_{2,3}$ absorption edge of these samples confirmed the anatase polymorph. A typical absorption spectrum is shown in Figure 4a (top). The spectrum is divided into four main peaks: the first two peaks (458 and 460 eV) correspond to the L_3 absorption edge and the last two peaks (463 and 465 eV) correspond to the L_2 edge. Both edges display two peaks because of the crystal field splitting in TiO_2.[57] The second peak, around 460 eV, is particularly broad with a shoulder on the high-energy side, typical of TiO_2 anatase[58] (see arrows Figure 4a).

Resonant photoemission is performed by tuning the photon energy from 450 to 480 eV and recording the photoelectron spectra of the VB region (BE ranging from 15 eV to the Fermi edge FE). Given that the photon energy matches the absorption edge of Ti, the VB photoemission is enhanced in the Ti-derived electron states. We referred to previous studies[59,60] comparing anatase and rutile to rescale in energy the XPS spectra and the XAS spectrum. Thus, all photoemission spectra have been rescaled in energy, considering the
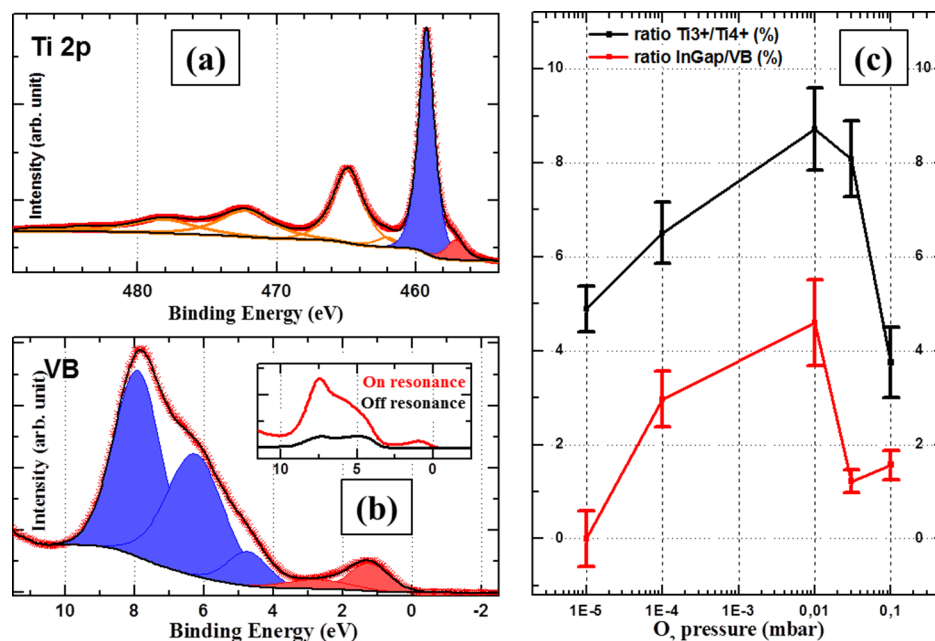
Figure 5. (a) Example of fit of the Ti 2p XPS peak obtained with a photon energy of 610 eV showing the main Ti $2p_{3/2}$ environment (Ti^{4+}, blue) and the suboxide environment (Ti^{3+}, red) obtained for a sample grown with an oxygen pressure of 10^{-2} mbar. (b) Fit of the resonant VB with three peaks in the VB (blue) and the in-gap state (red). The resonant VB is the difference between the VB at resonance (photon energy = 464 eV) and off resonance (photon energy = 450 eV) (red and black curves, respectively, in the top right inset). (c) General evolution of the presence of the Ti^{3+} environment (shown by the ratio Ti^{3+}/Ti^{4+} extracted from the Ti 2p XPS peak; black) and the in-gap state (extracted from the ratio between the intensity of the in-gap electronic state and the total VB area; red) as a function of the growth oxygen pressure.

Fermi edge at the CBM [because the band gap of anatase is 3.2 eV, the valence band minimum (VBM) is at a BE of 3.2 eV] and considering the Ti 2p main peak at a BE of 456.2 eV with respect to the VBM. As for the XAS spectrum, it has been rescaled considering the L$_3$ first sharp peak at 458 eV as comparable to the literature. In ResPES, both XAS and XPS are measured at the same time ensuring total correlation between the two scales and hence the correct resonant energies (see Figure 4a,b).

The overall energy resolution (photon bandpass and electron energy analyzer Omicron EA125) was set to 500 meV for XPS and ResPES. The results are shown in Figure 4b. The VB resonant photoemission shows extra electronic states located above the VBM within the gap, confirming previous reports on both rutile[61] and anatase.[41,62]

Our graph (Figure 4b) focuses on the region between VBM (BE = 3.2 eV) and FE (BE = 0). The XAS spectrum is added (red) with the position of the L$_2$ and L$_3$ edges indicated as references. The in-gap state, attributed in literature to the Ti^{3+} states due to O vacancies, is situated around 1.25 eV, in agreement with previous reports.[63,64] The intensity evolution of the in-gap state as a function of the photon energy [CIS curve, here in purple] is plotted together with the XAS spectrum (Figure 4a), showing two resonant energies at the position of the L$_3$ edge (~459 eV) and of the L$_2$ one (~464 eV). Because the in-gap state originates from the defect states, the electronic environment is different from bulk Ti atoms; thus, the CIS curve does not reflect the same behavior as the XAS curve, as reported in the literature.[40,65]

To probe the band dispersion of the in-gap states, ARPES experiments were performed on the in situ transferred TiO$_2$ sample. These experiments were carried out with a Scienta DA30 hemispherical electron energy and momentum analyzer with an overall 30° angular acceptance, which allows performing the band mapping over the extended areas of the Brillouin zone without sample rotation. ARPES experiments were performed at room temperature on as-grown TiO$_2$ thin films at a resonant photon energy of 45−50 eV (corresponding to the Ti 3p absorption edge[41]). The overall energy resolution was set to 100 meV, and the angular resolution was set to 0.2°. Figure 4c shows the ARPES VB dispersion of the anatase TiO$_2$

thin film, which is clearly visible in the 4−9 eV BE range. Although the top panel shows apparently no intensity within the gap (0−4 eV), the zoomed-in image in the bottom left panel (green rectangle in the top panel) reveals the presence of the in-gap nondispersive electronic defect state at BE = 1.5 eV, as deduced from the peak position in the angle integrated spectrum (Figure 4c, bottom right).

3. RESULTS AND DISCUSSION

The in-gap states observed in ARPES show no dispersion, which is a clear indication of their localized nature. We now address the origin of these defect states.

We first compare the electronic properties of TiO$_2$ thin films grown at different oxygen pressures, which should result in different amount of oxygen vacancies. Five anatase TiO$_2$ samples were grown at different oxygen pressures ranging from 10^{-1} to 10^{-5} mbar. The in-gap states visible at the L$_2$ edge energy (459 eV) and the Ti 2p photoelectron peak were considered to compare the in-gap state intensity with the Ti^{3+} environment. After subtraction of the Shirley background, the Ti 2p XPS experimental curves were fitted with six Gaussian−Lorentzian functions for taking into account the two main peaks (Ti$_{3/2}^{4+}$ and Ti$_{1/2}^{4+}$) and the four satellites typical of the Ti 2p peak in titanates such as SrTiO$_3$.[66] Two additional peaks were added on the low-energy side at the foot of the two main peaks to consider Ti^{3+} suboxides (see Figure 5a and more details in Figure S3). The ratio of the area of the peaks Ti$_{3/2}^{4+}$ (blue) and Ti$_{3/2}^{3+}$ (red) is measured for the different samples and displayed in Figure 5c (black curve) as a function of the growth oxygen pressure. In the same way, the VB is measured by photoemission using a photon energy of 464 eV (corresponding to the L$_2$ edge being the maximum of resonance of the in-gap state). A similar scan measured off resonance (450 eV) is subtracted to enhance the resonating states in the VB (inset in Figure 5b). Three Gaussian−

Lorentzian functions were used to fit the VB (blue). Two additional components were used to fit the in-gap state and the background increase in between VBM and the defect state (red). In the same way, the evolution of the ratio between the in-gap state intensity (red fit) and the VB intensity (blue fit) is taken into account as a function of the growth oxygen pressure (red curve in Figure 5c). The main graph (Figure 5c) is thus a direct comparison of the evolution of intensity of the Ti^{3+} electronic state and the intensity of the in-gap defect state. An error bar of 10% for the Ti^{3+}/Ti^{4+} ratio and 20% for the in-gap/VB ratio have been added to take into account experimental or data treatment uncertainties.

Results indicate a clear correlation between the amount of Ti^{3+} component and the intensity of the defect state. At very high oxygen pressure (10^{-1} mbar), the amount of detectable Ti^{3+} component with respect to the Ti^{4+} component drops. In the same way, we detect a very small intensity of the in-gap state in the VB spectrum. On the contrary, a much higher amount of the Ti^{3+} chemical environment and the in-gap state is measured for the sample grown at an oxygen pressure of 10^{-2} mbar. Interestingly and contrary to what is generally expected,[67,68] at lower oxygen growth pressure, we do not observe a continuous increase in the Ti^{3+} environment. Indeed, we observed a continuous decrease in the Ti^{3+} chemical environment correlated with a continuous decrease in the intensity of the in-gap defect state from 10^{-2} up to 10^{-5} mbar. Even though the oxygen background pressure is known to affect the expansion dynamics of the plasma and the average kinetic energy of the ablated species impinging on the substrate in a nontrivial way,[69] the nonmonotonic dependency of Ti^{3+} upon the oxygen deposition pressure is new because this is generally used for tuning the oxygen vacancies amount in oxide thin films. Taking into account that our results measure directly the Ti^{3+} chemical state and not the amount of oxygen vacancies, we assign the presence and evolution of the in-gap electronic states as a direct signature of the Ti^{3+} chemical environment, though we are not able to quantify the origin of such signature (oxygen vacancies and/or Ti^{3+} interstitial[23,28]). It is however clear from the results in Figure 5 that the oxygen growth pressure does not have a direct proportionality with the oxygen vacancies. Calculations[23] on anatase and rutile indicate similar activation energies for the two kinds of defects (O vacancies or Ti interstitials) and that growth conditions (temperature and oxygen pressure), as confirmed by present results, play an important role.

Furthermore, XPS measurements recorded on all of these samples at 900 eV (low photon energy and hence highly surface sensitive) show the presence of peaks of Al 2s and 2p of different intensities as a function of the sample growth pressure. As a matter of fact, the intensity of the Al 2p peaks shows a trend fully comparable with the Ti^{3+} component having the highest shown intensity of Al when the Ti^{3+} component is maximum (10^{-2} mbar, see Figures 3d and 5c) and a much smaller intensity when the Ti^{3+} component is low (10^{-1} and 10^{-4} mbar). The presence of Al all along the film thickness up to the surface with apparently a uniform dilution in the film is compatible with the presence of these shear planes that act as diffusion channels through the film[50] (Figure 2b shows the HRTEM image of the sample grown at an oxygen pressure of 10^{-2} mbar, showing the highest intensity of Ti^{3+} and the in-gap electronic state in Figure 5c). In addition, shear planes could also affect the presence of Ti^{3+} interstitials. All of these features could explain the nontrivial correlation between the Ti^{3+}

amount and the oxygen growth pressure. However, regardless of the origin of the Ti^{3+} environments in the film, a clear correlation has been established between Ti^{3+} and in-gap electronic states.

4. CONCLUSIONS

We performed a complete structural and spectroscopic characterization of PLD-grown $TiO_2(001)$-oriented anatase films. TiO_2 is a crucial material for potential application in photocatalysis, and the study of its electronic properties, especially in its anatase form, is of major interest. Our data affirm good crystalline quality of the films, relaxed lattice parameter, smooth surface, and typical (1×4) surface reconstruction. HRTEM experiments enlighten the nanostructural homogeneity of the films, which consists of anatase TiO_2 defective phases characterized by CS planes originating from the ordered arrays of oxygen vacancies. Selected TiO_2 thin films were characterized by a large range of in situ and ex situ spectroscopic techniques. The presence of the in-gap electronic state is confirmed by both ResPES and ARPES, and its localized nature is confirmed by the absence of electronic dispersion.

ResPES, XPS, and HAXPES of anatase thin films grown at different oxygen pressures show a clear correlation between the in-gap electronic state and the intensity of the Ti^{3+} component. However, no clear correlations between the oxygen growth pressure and the presence of these defect states are observed.

The presence of Al diffusing from the LAO substrate revealed by HAXPES and the presence of CS planes usually associated with the oxygen vacancies demonstrate the bulk rather than the surface character of these defect states.

The origin of the Ti^{3+} electronic states and their intensity evolution regarding growth conditions have to be investigated within the probable correlation between several parameters, including oxygen vacancy amount, shear plane stabilization, presence of Ti^{3+} interstitials, and Al diffusion. The disentanglement of influence of these different parameters on the origin and importance of the Ti^{3+} valence state would provide a deep insight into the particular electronic properties of TiO_2 anatase.

Our results refine the understanding of the defects at the origin of the in-gap electronic state and open the way to a better control of the specific surface properties of TiO_2 anatase through its growth conditions.

■ ASSOCIATED CONTENT

Ⓢ Supporting Information

The Supporting Information is available free of charge on the ACS Publications website at DOI: 10.1021/acsami.7b03181.

> Description of the sample surface characterization by LEED and STM, experimental results on the Ti 2p peak showing the Ti^{3+} environment as a function of the HAXPES probing depth, and detailed fitting procedure for the XPS Ti 2p peak and comparison of the different samples (PDF)

■ AUTHOR INFORMATION

Corresponding Author

*E-mail: benoit.gobaut@synchrotron-soleil.fr.

ORCID Ⓘ

Benoit Gobaut: 0000-0002-4086-8774

Pasquale Orgiani: 0000-0002-1082-9651

Carmela Aruta: 0000-0002-6917-6667

Fabio Miletto Granozio: 0000-0002-9417-7848
Present Address
††Synchrotron SOLEIL, L'Orme des Merisiers, 91192 Saint-Aubin, France (B.G.).

Author Contributions
The manuscript was written through contributions of all authors. All authors have given approval to the final version of the manuscript.

Notes
The authors declare no competing financial interest.

■ REFERENCES

(1) Diebold, U. The Surface Science of Titanium Dioxide. *Surf. Sci. Rep.* **2003**, *48*, 53−229.

(2) Fujishima, A.; Zhang, X.; Tryk, D. A. TiO$_2$ Photocatalysis and Related Surface Phenomena. *Surf. Sci. Rep.* **2008**, *63*, 515−582.

(3) Henderson, M. A. A Surface Science Perspective on TiO$_2$ Photocatalysis. *Surf. Sci. Rep.* **2011**, *66*, 185−297.

(4) Fujishima, A.; Honda, K. Electrochemical Photolysis of Water at a Semiconductor Electrode. *Nature* **1972**, *238*, 37−38.

(5) Mills, A.; Davies, R. H.; Worsley, D. Water Purification by Semiconductor Photocatalysis. *Chem. Soc. Rev.* **1993**, *22*, 417.

(6) Rosseler, O.; Sleiman, M.; Montesinos, V. N.; Shavorskiy, A.; Keller, V.; Keller, N.; Litter, M. I.; Bluhm, H.; Salmeron, M.; Destaillats, H. Chemistry of NO$_x$ on TiO$_2$ Surfaces Studied by Ambient Pressure XPS: Products, Effect of UV Irradiation, Water, and Coadsorbed K$^+$. *J. Phys. Chem. Lett.* **2013**, *4*, 536−541.

(7) Hashimoto, K.; Irie, H.; Fujishima, A. Photocatalysis: A Historical Overview and Future Prospects. *Jpn. J. Appl. Phys., Part 1* **2005**, *44*, 8269−8285.

(8) Jribi, R.; Barthel, E.; Bluhm, H.; Grunze, M.; Koelsch, P.; Verreault, D.; Søndergård, E. Ultraviolet Irradiation Suppresses Adhesion on TiO$_2$. *J. Phys. Chem. C* **2009**, *113*, 8273−8277.

(9) O'Regan, B.; Grätzel, M. A Low-Cost, High-Efficiency Solar Cell Based on Dye-Sensitized Colloidal TiO$_2$ Films. *Nature* **1991**, *353*, 737−740.

(10) Jeong, H. Y.; Lee, J. Y.; Choi, S.-Y. Interface-Engineered Amorphous TiO$_2$-Based Resistive Memory Devices. *Adv. Funct. Mater.* **2010**, *20*, 3912−3917.

(11) Regoutz, A.; Gupta, I.; Serb, A.; Khiat, A.; Borgatti, F.; Lee, T.-L.; Schlueter, C.; Torelli, P.; Gobaut, B.; Light, M.; Carta, D.; Pearce, S.; Panaccione, G.; Prodromakis, T. Role and Optimization of the Active Oxide Layer in TiO$_2$-Based RRAM. *Adv. Funct. Mater.* **2016**, *26*, 507−513.

(12) Guo, Q.; Zhou, C.; Ma, Z.; Ren, Z.; Fan, H.; Yang, X. Elementary Photocatalytic Chemistry on TiO$_2$ Surfaces. *Chem. Soc. Rev.* **2016**, *45*, 3701−3730.

(13) Boddy, P. J. Oxygen Evolution on Semiconducting TiO$_2$. *J. Electrochem. Soc.* **1968**, *115*, 199−203.

(14) Zhang, J.; Zhou, P.; Liu, J.; Yu, J. New Understanding of the Difference of Photocatalytic Activity among Anatase, Rutile and Brookite TiO$_2$. *Phys. Chem. Chem. Phys.* **2014**, *16*, 20382−20386.

(15) Setvin, M.; Franchini, C.; Hao, X.; Schmid, M.; Janotti, A.; Kaltak, M.; van de Walle, C. G.; Kresse, G.; Diebold, U. Direct View at Excess Electrons in TiO$_2$ Rutile and Anatase. *Phys. Rev. Lett.* **2014**, *113*, 086402.

(16) Luttrell, T.; Halpegamage, S.; Tao, J.; Kramer, A.; Sutter, E.; Batzill, M. Why is Anatase a Better Photocatalyst than Rutile?−Model Studies on Epitaxial TiO$_2$ Films. *Sci. Rep.* **2014**, *4*, 4043.

(17) Bear, J. C.; Gomez, V.; Kefallinos, N. S.; McGettrick, J. D.; Barron, A. R.; Dunnill, C. W. Anatase/rutile Bi-Phasic Titanium Dioxide Nanoparticles for Photocatalytic Applications Enhanced by Nitrogen Doping and Platinum Nano-Islands. *J. Colloid Interface Sci.* **2015**, *460*, 29−35.

(18) Gong, X.-Q.; Selloni, A. Reactivity of Anatase TiO$_2$ Nanoparticles: The Role of the Minority (001) Surface. *J. Phys. Chem. B* **2005**, *109*, 19560−19562.

(19) Forro, L.; Chauvet, O.; Emin, D.; Zuppiroli, L.; Berger, H.; Lévy, F. High Mobility n-Type Charge Carriers in Large Single Crystals of Anatase (TiO$_2$). *J. Appl. Phys.* **1994**, *75*, 633.

(20) Sarkar, T.; Gopinadhan, K.; Zhou, J.; Saha, S.; Coey, J. M. D.; Feng, Y. P.; Ariando; Venkatesan, T. Electron Transport at the TiO$_2$ Surfaces of Rutile, Anatase, and Strontium Titanate: The Influence of Orbital Corrugation. *ACS Appl. Mater. Interfaces* **2015**, *7*, 24616−24621.

(21) Tang, H.; Berger, H.; Schmid, P. E.; Lévy, F.; Burri, G. Photoluminescence in TiO$_2$ Anatase Single Crystals. *Solid State Commun.* **1993**, *87*, 847−850.

(22) Kavan, L.; Grätzel, M.; Gilbert, S. E.; Klemenz, C.; Scheel, H. J. Electrochemical and Photoelectrochemical Investigation of Single-Crystal Anatase. *J. Am. Chem. Soc.* **1996**, *118*, 6716−6723.

(23) Morgan, B. J.; Watson, G. W. Intrinsic N-Type Defect Formation in TiO$_2$: A Comparison of Rutile and Anatase from GGA+U Calculations. *J. Phys. Chem. C* **2010**, *114*, 2321−2328.

(24) Portillo-Vélez, N. S.; Olvera-Neria, O.; Hernández-Pérez, I.; Rubio-Ponce, A. Localized Electronic States Induced by Oxygen Vacancies on Anatase TiO$_2$(101) Surface. *Surf. Sci.* **2013**, *616*, 115−119.

(25) Setvin, M.; Aschauer, U.; Scheiber, P.; Li, Y.-F.; Hou, W.; Schmid, M.; Selloni, A.; Diebold, U. Reaction of O$_2$ with Subsurface Oxygen Vacancies on TiO$_2$ Anatase (101). *Science* **2013**, *341*, 988−991.

(26) He, Y.; Dulub, O.; Cheng, H.; Selloni, A.; Diebold, U. Evidence for the Predominance of Subsurface Defects on Reduced Anatase TiO$_2$(101). *Phys. Rev. Lett.* **2009**, *102*, 106105.

(27) Diebold, U.; Ruzycki, N.; Herman, G. S.; Selloni, A. One Step towards Bridging the Materials Gap: Surface Studies of TiO$_2$ Anatase. *Catal. Today* **2003**, *85*, 93−100.

(28) Wendt, S.; Sprunger, P. T.; Lira, E.; Madsen, G. K. H.; Li, Z.; Hansen, J. Ø.; Matthiesen, J.; Blekinge-rasmussen, A.; Laegsgaard, E.; Hammer, B.; Besenbacher, F. The Role of Interstitial Sites in the Ti3d Defect State in the Band Gap of Titania. *Science* **2008**, *320*, 1755−1759.

(29) Tao, J.; Luttrell, T.; Batzill, M. A Two-Dimensional Phase of TiO$_2$ with a Reduced Bandgap. *Nat. Chem.* **2011**, *3*, 296−300.

(30) Gong, X.-Q.; Selloni, A.; Batzill, M.; Diebold, U. Steps on Anatase TiO$_2$(101). *Nat. Mater.* **2006**, *5*, 665−670.

(31) Padilha, A. C. M.; Raebiger, H.; Rocha, A. R.; Dalpian, G. M. Charge Storage in Oxygen Deficient Phases of TiO$_2$: Defect Physics without Defects. *Sci. Rep.* **2016**, *6*, 28871.

(32) Yoshimatsu, K.; Sakata, O.; Ohtomo, A. Superconductivity in Higher Titanium Oxides. **2016**, arXiv:1612.02502.

(33) Krupski, K.; Sanchez, A. M.; Krupski, A.; McConville, C. F. Optimisation of Anatase TiO$_2$ Thin Film Growth on LaAlO$_3$(001) Using Pulsed Laser Deposition. *Appl. Surf. Sci.* **2016**, *388*, 684−690.

(34) Vasu, K.; Sreedhara, M. B.; Ghatak, J.; Rao, C. N. R. Atomic Layer Deposition of p-Type Epitaxial Thin Films of Undoped and N-Doped Anatase TiO$_2$. *ACS Appl. Mater. Interfaces* **2016**, *8*, 7897−7901.

(35) Papageorgiou, A. C.; Beglitis, N. S.; Pang, C. L.; Teobaldi, G.; Cabailh, G.; Chen, Q.; Fisher, A. J.; Hofer, W. A.; Thornton, G. Electron Traps and Their Effect on the Surface Chemistry of TiO$_2$(110). *Proc. Natl. Acad. Sci. U.S.A.* **2010**, *107*, 2391−2396.

(36) Yim, C. M.; Pang, C. L.; Thornton, G. Oxygen Vacancy Origin of the Surface Band-Gap State of TiO$_2$(110). *Phys. Rev. Lett.* **2010**, *104*, 036806.

(37) Wang, Y.; Sun, H.; Tan, S.; Feng, H.; Cheng, Z.; Zhao, J.; Zhao, A.; Wang, B.; Luo, Y.; Yang, J.; Hou, J. G. Role of Point Defects on the Reactivity of Reconstructed Anatase Titanium Dioxide (001) Surface. *Nat. Commun.* **2013**, *4*, 2214.

(38) Zhang, Z.; Jeng, S.-P.; Henrich, V. E. Cation-Ligand Hybridization for Stoichiometric and Reduced TiO_2 (110) Surfaces Determined by Resonant Photoemission. *Phys. Rev. B: Condens. Matter Mater. Phys.* **1991**, *43*, 12004−12011.

(39) Sanjinés, R.; Tang, H.; Berger, H.; Gozzo, F.; Margaritondo, G.; Lévy, F. Electronic Structure of Anatase TiO_2 Oxide. *J. Appl. Phys.* **1994**, *75*, 2945−2951.

(40) Prince, K. C.; Dhanak, V. R.; Finetti, P.; Walsh, J. F.; Davis, R.; Muryn, C. A.; Dhariwal, H. S.; Thornton, G.; van der Laan, G. 2p Resonant Photoemission Study of TiO_2s. *Phys. Rev. B: Condens. Matter Mater. Phys.* **1997**, *55*, 9520−9523.

(41) Thomas, A. G.; Flavell, W. R.; Kumarasinghe, A. R.; Mallick, A. K.; Tsoutsou, D.; Smith, G. C.; Stockbauer, R.; Patel, S.; Grätzel, M.; Hengerer, R. Resonant Photoemission of Anatase TiO_2(101) and (001) Single Crystals. *Phys. Rev. B: Condens. Matter Mater. Phys.* **2003**, *67*, 035110.

(42) Krüger, P.; Bourgeois, S.; Domenichini, B.; Magnan, H.; Chandesris, D.; Le Fèvre, P.; Flank, A. M.; Jupille, J.; Floreano, L.; Cossaro, A.; Verdini, A.; Morgante, A. Defect States at the TiO_2(110) Surface Probed by Resonant Photoelectron Diffraction. *Phys. Rev. Lett.* **2008**, *100*, 055501.

(43) Choi, J.; Eom, C. B.; Rijnders, G.; Rogalla, H.; Blank, D. H. A. Growth Mode Transition from Layer by Layer to Step Flow during the Growth of Heteroepitaxial $SrRuO_3$ on (001) $SrTiO_3$. *Appl. Phys. Lett.* **2001**, *79*, 1447−1449.

(44) Kennedy, R. J.; Stampe, P. A. The Influence of Lattice Mismatch and Film Thickness on the Growth of TiO_2 on $LaAlO_3$ and $SrTiO_3$ Substrates. *J. Cryst. Growth* **2003**, *252*, 333−342.

(45) Lazzeri, M.; Selloni, A. Stress-Driven Reconstruction of an Oxide Surface: The Anatase TiO_2(001) − (1 × 4) Surface. *Phys. Rev. Lett.* **2001**, *87*, 266105.

(46) Liang, Y.; Gan, S.; Chambers, S. A.; Altman, E. I. Surface Structure of Anatase TiO_2(001): Reconstruction, Atomic Steps, and Domains. *Phys. Rev. B: Condens. Matter Mater. Phys.* **2001**, *63*, 235402.

(47) Hengerer, R.; Bolliger, B.; Erbudak, M.; Grätzel, M. Structure and Stability of the Anatase TiO2 (101) and (001) Surfaces. *Surf. Sci.* **2000**, *460*, 162−169.

(48) Panaccione, G.; Vobornik, I.; Fujii, J.; Krizmancic, D.; Annese, E.; Giovanelli, L.; Maccherozzi, F.; Salvador, F.; De Luisa, A.; Benedetti, D.; Gruden, A.; Bertoch, P.; Polack, F.; Cocco, D.; Sostero, G.; Diviacco, B.; Hochstrasser, M.; Maier, U.; Pescia, D.; Back, C. H.; Greber, T.; Osterwalder, J.; Galaktionov, M.; Sancrotti, M.; Rossi, G. Advanced Photoelectric Effect Experiment Beamline at Elettra: A Surface Science Laboratory Coupled with Synchrotron Radiation. *Rev. Sci. Instrum.* **2009**, *80*, 043105.

(49) Ciancio, R.; Carlino, E.; Rossi, G.; Aruta, C.; di Uccio, U. S.; Vittadini, A.; Selloni, A. Magnéli-like Phases in Epitaxial Anatase TiO_2 Thin Films. *Phys. Rev. B: Condens. Matter Mater. Phys.* **2012**, *86*, 104110.

(50) Ciancio, R.; Carlino, E.; Aruta, C.; Maccariello, D.; Granozio, F. M.; di Uccio, U. S. Nanostructure of Buried Interface Layers in TiO_2 Anatase Thin Films Grown on $LaAlO_3$ and $SrTiO_3$ Substrates. *Nanoscale* **2012**, *4*, 91−94.

(51) Rueff, J.-P.; Ablett, J. M.; Céolin, D.; Prieur, D.; Moreno, T.; Balédent, V.; Lassalle-Kaiser, B.; Rault, J. E.; Simon, M.; Shukla, A. The GALAXIES Beamline at the SOLEIL Synchrotron: Inelastic X-Ray Scattering and Photoelectron Spectroscopy in the Hard X-Ray Range. *J. Synchrotron Radiat.* **2015**, *22*, 175−179.

(52) Sacchi, M.; Offi, F.; Torelli, P.; Fondacaro, A.; Spezzani, C.; Cautero, M.; Cautero, G.; Huotari, S.; Grioni, M.; Delaunay, R.; Fabrizioli, M.; Vankó, G.; Monaco, G.; Paolicelli, G.; Stefani, G.; Panaccione, G. Quantifying the Effective Attenuation Length in High-Energy Photoemission Experiments. *Phys. Rev. B: Condens. Matter Mater. Phys.* **2005**, *71*, 155117.

(53) Radović, M.; Salluzzo, M.; Ristić, Z.; Di Capua, R.; Lampis, N.; Vaglio, R.; Granozio, F. M. In Situ Investigation of the Early Stage of TiO_2 Epitaxy on (001) $SrTiO_3$. *J. Chem. Phys.* **2011**, *135*, 034705.

(54) Borgatti, F.; Park, C.; Herpers, A.; Offi, F.; Egoavil, R.; Yamashita, Y.; Yang, A.; Kobata, M.; Kobayashi, K.; Verbeeck, J.; Panaccione, G.; Dittmann, R. Chemical Insight into Electroforming of Resistive Switching Manganite Heterostructures. *Nanoscale* **2013**, *5*, 3954−3960.

(55) Sing, M.; Berner, G.; Goß, K.; Müller, A.; Ruff, A.; Wetscherek, A.; Thiel, S.; Mannhart, J.; Pauli, S. A.; Schneider, C. W.; Willmott, P. R.; Gorgoi, M.; Schäfers, F.; Claessen, R. Profiling the Interface Electron Gas of $LaAlO_3/SrTiO_3$ Heterostructures with Hard X-Ray Photoelectron Spectroscopy. *Phys. Rev. Lett.* **2009**, *102*, 176805.

(56) Treske, U.; Heming, N.; Knupfer, M.; Büchner, B.; Di Gennaro, E.; Khare, A.; Di Uccio, U. S.; Granozio, F. M.; Krause, S.; Koitzsch, A. Universal Electronic Structure of Polar Oxide Hetero-Interfaces. *Sci. Rep.* **2015**, *5*, 14506.

(57) de Groot, F. M. F.; Fuggle, J. C.; Thole, B. T.; Sawatzky, G. A. $L_{2,3}$ X-Ray Absorption Edges of d^0 Compounds: K^+, Ca^{2+}, Sc^{3+}, and Ti^{4+} in O_h (Octahedral) Symmetry. *Phys. Rev. B: Condens. Matter Mater. Phys.* **1990**, *41*, 928−937.

(58) Stoyanov, E.; Langenhorst, F.; Steinle-Neumann, G. The Effect of Valence State and Site Geometry on Ti $L_{3,2}$ and O K Electron Energy-Loss Spectra of Ti_xO_y Phases. *Am. Mineral.* **2007**, *92*, 577−586.

(59) Pfeifer, V.; Erhart, P.; Li, S.; Rachut, K.; Morasch, J.; Brötz, J.; Reckers, P.; Mayer, T.; Rühle, S.; Zaban, A.; Seró, I. M.; Bisquert, J.; Jaegermann, W.; Klein, A. Energy Band Alignment between Anatase and Rutile TiO_2. *J. Phys. Chem. Lett.* **2013**, *4*, 4182−4187.

(60) Deák, P.; Kullgren, J.; Aradi, B.; Frauenheim, T.; Kavan, L. Water Splitting and the Band Edge Positions of TiO_2. *Electrochim. Acta* **2016**, *199*, 27−34.

(61) Drera, G.; Sangaletti, L.; Bondino, F.; Malvestuto, M.; Malavasi, L.; Diaz-Fernandez, Y.; Dash, S.; Mozzati, M. C.; Galinetto, P. Labeling Interacting Configurations through an Analysis of Excitation Dynamics in a Resonant Photoemission Experiment: The Case of Rutile TiO_2. *J. Phys.: Condens. Matter* **2013**, *25*, 075502.

(62) Thomas, A. G.; Flavell, W. R.; Mallick, A. K.; Kumarasinghe, A. R.; Tsoutsou, D.; Khan, N.; Chatwin, C.; Rayner, S.; Smith, G. C.; Stockbauer, R. L.; Warren, S.; Johal, T. K.; Patel, S.; Holland, D.; Taleb, A.; Wiame, F. Comparison of the Electronic Structure of Anatase and Rutile TiO_2 Single-Crystal Surfaces Using Resonant Photoemission and X-Ray Absorption Spectroscopy. *Phys. Rev. B: Condens. Matter Mater. Phys.* **2007**, *75*, 035105.

(63) Reckers, P.; Dimamay, M.; Klett, J.; Trost, S.; Zilberberg, K.; Riedl, T.; Parkinson, B. A.; Brötz, J.; Jaegermann, W.; Mayer, T. Deep and Shallow TiO_2 Gap States on Cleaved Anatase Single Crystal (101) Surfaces, Nanocrystalline Anatase Films, and ALD Titania Ante and Post Annealing. *J. Phys. Chem. C* **2015**, *119*, 9890−9898.

(64) Miccio, L. A.; Setvin, M.; Müller, M.; Abadía, M.; Piquero, I.; Lobo-Checa, J.; Schiller, F.; Rogero, C.; Schmid, M.; Sánchez-Portal, D.; Diebold, U.; Ortega, J. E. Interplay between Steps and Oxygen Vacancies on Curved TiO_2(110). *Nano Lett.* **2016**, *16*, 2017−2022.

(65) Caruso, T.; Lenardi, C.; Agostino, R. G.; Amati, M.; Bongiorno, G.; Mazza, T.; Policicchio, A.; Formoso, V.; Maccallini, E.; Colavita, E.; Chiarello, G.; Finetti, P.; Šutara, F.; Skála, T.; Piseri, P.; Prince, K. C.; Milani, P. Electronic Structure of Cluster Assembled Nanostructured TiO_2 by Resonant Photoemission at the Ti $L_{2,3}$ Edge. *J. Chem. Phys.* **2008**, *128*, 094704.

(66) Woicik, J. C.; Weiland, C.; Rumaiz, A. K. Loss for Photoemission versus Gain for Auger: Direct Experimental Evidence of Crystal-Field Splitting and Charge Transfer in Photoelectron Spectroscopy. *Phys. Rev. B: Condens. Matter Mater. Phys.* **2015**, *91*, 201412.

(67) Ali, B.; Rumaiz, A. K.; Ozbay, A.; Nowak, E. R.; Shah, S. I. Influence of Oxygen Partial Pressure on Structural, Transport and Magnetic Properties of Co Doped Films. *Solid State Commun.* **2009**, *149*, 2210−2214.

(68) Lee, H. N.; Seo, S. S. A.; Choi, W. S.; Rouleau, C. M. Growth Control of Oxygen Stoichiometry in Homoepitaxial $SrTiO_3$ Films by Pulsed Laser Epitaxy in High Vacuum. *Sci. Rep.* **2016**, *6*, 19941.

(69) Sambri, A.; Amoruso, S.; Wang, X.; Granozio, F. M.; Bruzzese, R. Plume Propagation Dynamics of Complex Oxides in Oxygen. *J. Appl. Phys.* **2008**, *104*, 053304.